applied sciences

MDPI

Article

Lignocellulosic Materials Used as Biosorbents for the Capture of Nickel (II) in Aqueous Solution

Luísa Cruz-Lopes [1,*], Morgana Macena [1], Bruno Esteves [1] and Isabel Santos-Vieira [2]

[1] CERNAS Research Centre, School of Technology and Management, Polytechnic Institute of Viseu, 3504-510 Viseu, Portugal; estgv17498@alunos.estgv.ipv.pt (M.M.); bruno@estgv.ipv.pt (B.E.)
[2] CICECO—Aveiro Institute of Materials, Department of Chemistry, University of Aveiro, 3810-193 Aveiro, Portugal; ivieira@ua.pt
* Correspondence: lvalente@estgv.ipv.pt

Abstract: Four lignocellulosic materials (walnut shell, chestnut shell, pine wood and burnt pine wood) were analyzed as biosorbents to remove nickel ions in aqueous solution. The optimal pH condition was determined. Due to this, a range of different pHs (3.0 to 7.5) was tested. The adsorption isotherms and kinetics were established. To plot Langmuir and Freundlich isotherms, batch adsorption tests were made with variable nickel concentrations (5 to 200 mg L^{-1}). The pseudo-first order, pseudo-second order, Elovich and intraparticle diffusion models were used to describe the kinetics, batch adsorption tests were carried out with 25 mg L^{-1} of nickel solution and agitation time varied from 10 to 1440 min. The specific surface area of the different materials was between 3.97 and 4.85 m^2g^{-1} with the exception for wood with 1.74 m^2g^{-1}. The pore size was 26.54 nm for wood and varied between 5.40 and 7.33 nm for the remaining materials. The diffractograms analysis showed that all the lignocellulosic materials presented some crystalline domains with the exception of burnt pine wood which was completely amorphous. The best pH was found to be around 5.0. At this pH the adsorption was higher for chestnut shells, walnut shells, burnt pine wood and wood, respectively. All samples fitted the Langmuir model well, with R^2 of 0.994 to 0.998. The sorption kinetics was well described by the pseudo-second order equation with R^2 between 0.996 and 1.00. No significative differences on the surface of the materials before and after adsorption could be observed by SEM. Finally, all materials tested were able to remove nickel ions in aqueous solution.

Keywords: BET; biosorbents; isotherms; kinetics; lignocellulosic materials; nickel; SEM; XRD

Citation: Cruz-Lopes, L.; Macena, M.; Esteves, B.; Santos-Vieira, I. Lignocellulosic Materials Used as Biosorbents for the Capture of Nickel (II) in Aqueous Solution. *Appl. Sci.* **2022**, *12*, 933. https://doi.org/10.3390/app12020933

Academic Editor: Alenka Temeljotov-Salaj

Received: 13 December 2021
Accepted: 11 January 2022
Published: 17 January 2022

1. Introduction

A current environmental issue is the pollution of water resources which occurs mostly due to the disposal of contaminated industrial wastewater [1]. The existence of contaminant compounds in water, especially drinking water, is of considerable risk to the environment and consumers [2]. Among the toxic metals currently found in industrial wastewaters, nickel is one of the most common [3]. According to Decree-Law No. 236/98 of 1 August of the Ministry of Environment, the maximum limit value for the discharge of wastewater containing nickel is 2.0 mg/L [4].

Various industries such as mineral processing, electroplating and production of paints and batteries employ nickel in their activities [5]. Several negative effects may occur when people are exposed to a high concentration of nickel, which means the polluted environment also affects human health. Heavy metals are one of the most dangerous pollutants. When in aquatic environments, even in low concentrations, they represent a risk to the ecosystem sustainability [1].

The use of nickel in several materials used in our daily life contributes to a greater contact with this metal. The most common effect produced by direct contact with nickel is dermatitis, being one of the main precursors of allergic contact dermatitis [6]. Carbonyl

is the compound of nickel most toxic to humans [7]. The ingestion of nickel can cause inhibition of enzyme activities, damage to the lungs and kidneys, gastrointestinal disease and respiratory problems [8].

Adsorption methods have been attracting significant interest during recent years [9]. The treatment of heavy metals in wastewater using adsorption is making progress through research focused on the development of highly efficient materials, with low cost as well as eco-friendly adsorbents [10]. Alternative materials such as byproducts of agricultural processes have been evaluated due to their efficiency, availability and accessibility [11]. There are many potential biosorbent materials that have been tested to determinate their application in adsorption processes. These materials should have, among other characteristics, high surface area, selectivity, sorption capacity and compatibility with the contaminant and the process [12].

Agricultural biomass residues generally consist of cellulose, lignin, hemicelluloses and proteins which make them successful adsorbents to remove heavy metals [13]. Some studies presented good results by using different biomasses in the decontamination of aquatic environments, and potential biosorbents were discovered. Activated carbons produced by cassava peel, which was applied to remove dyes and metal ions from aqueous solution at various pHs, with adsorption rates from 5.30 to 100%, is one example [14]. Residues from *Jatropha curcas* were used as biosorbent for the removal of Remazol Brilliant Blue R; the highest removal rate was around 95% at pH 3.0 [15]. *Pinus elliottii* bark was tested as adsorbent to remove heavy metals such as cadmium, lead and chromium; the uptake was around 90% for all metals tested at pH 5.0 and 7.0 [16]. Heat-treated wood (powdered pine wood) was employed as chromium adsorbent, and the maximum retention was 15.6 to 19.4 mg g^{-1} at pH 3 [17].

Activated carbon is the most used adsorbent due to its high specific surface area which can reach almost 2000 m^2g^{-1} as reported before [18,19]. Several authors reported the specific surface area of different lignocellulosic materials such as coconut dregs residue with 0.38 m^2/g [20], husks of water bamboo (*Zizania caduciflora* Turcz.), with surface area of 1.87 m^2/g [21], chestnut shell with 7.01 m^2/g [22] or *Cryptomeria japonica* wood with 90–145 m^2/g [23]. Nevertheless, even though lignocellulosic materials have a much lower specific surface area, they are much cheaper and can be discharged after use.

Some activated carbons prepared with dried fruit, such as almonds, hazelnuts, walnuts and apricot kernels, are good adsorbents, as they have high surface area and well-developed micropores [24]. In the same way, the processing of wood generates a large volume of waste, so the implementation of this waste in adsorption processes has been advantageous, as it allows the use of these secondary materials [25]. Thus, the application of biosorbents in wastewater treatment results in lower cost and reduced environmental impact.

Lignocellulosic materials such as rice bran [5], rice husk [9] and sugarcane bagasse [10] have been tested to treat water contaminated with nickel. The study of novel materials with adsorbent potential, especially to remove nickel ions in aqueous media, seems to be very important since the use of biosorbents reduces the costs of the treatment and represents a solution to the issue of discharge of the residues from agriculture.

This study consists of the evaluation of four lignocellulosic materials used as biosorbent to remove nickel ions (Ni^{2+}) in aqueous solution: walnut shell (*Carya illinoensis* (Wangenh.) K.Koch.), chestnut shell (*Castanea sativa* Mill), pine wood (*Pinus* spp.) and burnt pine wood (*Pinus* spp.). In addition, the pH was tested to obtain optimal solution conditions. The isotherms of adsorption were analyzed using Langmuir and Freundlich equations; moreover, the reaction kinetics was also studied by applying the pseudo-first order, pseudo-second order, Elovich and intraparticle diffusion models.

2. Materials and Methods

2.1. Materials

Walnut shells and chestnut shells came from Transagri, Lda, a company in the Mangualde area, Viseu; this is a dry fruits company that generally uses them in a furnace. Burnt pine wood came from our local forest that has suffered a number of wildfires in the last few years, leading to burnt pine wood being left rotting in the fields. Pine wood was used for comparison purposes. The lignocellulosic materials tested were milled (Retsch SMI mill) and sieved (Retsch AS200) for 20 min at a speed of 50 rpm. Four fractions were obtained: 40 mesh (>0.420 mm); 40–60 mesh (0.420–0.250 mm); 60–80 mesh (0.250–0.177 mm); and <80 mesh (<0.177 mm). The fraction used in this study as adsorbent was the powder (<80 mesh), which was dried for 24 h at 105 in an oven.

A stock solution of nickel ($NiCl_2 \cdot 6H_2O$ with distilled water) with a concentration of 1000 mg L^{-1} was prepared.

2.2. Characterization

Nitrogen adsorption−desorption isotherms at 77 K were measured on a Micrometrics Gemini V2.0 (Micromeritics Instrument Corp.) system. All samples were pre-treated overnight at 473 K under nitrogen before measurements. The pore size was calculated from desorption branches of isotherms by the Barrett–Joyner–Halenda (BJH) method. Surface areas were calculated by the Brunauer–Emmett–Teller (BET) method.

FTIR-ATR spectra were made in a Perkin Elmer UATR Spectrum Two spectrometer with 72 scans/min with a resolution of 4.0 cm−1 over the 4000 to 400 cm−1 range for the initial materials and after nickel adsorption in a 25 mg L^{-1} solution. The samples were dried in an oven at 100 °C before FTIR-ATR testing. The spectrum was obtained after performing the background, placing the sample powder over the crystal and pressing it against the crystal. The average of three spectra was used.

Powder X-ray diffraction (PXRD) data were collected at ambient temperature on an Empyrean PANalytical diffractometer, with a working wavelength of λ1 = 1.540598 Å and λ2 = 1.544426 Å (Cu Kα1,2 X-radiation), equipped with a PIXcel 1D detector and a flat-plate sample holder in a Bragg–Brentano para-focusing optics configuration (45 kV, 40 mA). Intensity data were collected by the step-counting method (step 0.01°), in continuous mode, in the $3.5° \leq 2\theta° \leq 50°$ range.

Scanning electron microscopy (SEM) was carried out on a high-resolution Hitachi SU-70 (Monocomp) working at 15 kV. Samples were prepared by deposition on aluminum sample holders followed by carbon coating using an Emitech K950X carbon evaporator.

2.3. pH Optimization

A range of different pHs (3.0 to 7.5) was tested to obtain an ideal pH, suitable for the materials under evaluation. NaOH and HCl solutions (0.1 mol) were used for pH adjustment. The analyses were performed for each biosorbent using three replicates, containing 25 mL of solution with a metal concentration of 200 mg L^{-1} and 100 mg of adsorbent, which remained under constant stirring for 12 h in a shaker at room temperature. The containers were covered with aluminum foil to prevent evaporation. After the agitation period, the samples were filtered with paper filter by gravity. Spectrophotometry of atomic absorption by flame was used to evaluate the nickel sorption.

2.4. Adsorption Isotherms

To plot Langmuir and Freundlich equilibrium isotherms, adsorption tests were made with variable nickel concentrations from 5 to 200 mg L^{-1} and 100 mg of adsorbent. The tests were carried out in the same manner at the same pH. The parameters were determined by the linearized equations.

The Langmuir linear isotherm can be written as:

$$\frac{1}{q_e} = \frac{1}{q_{max}} + \left(\frac{1}{K_L q_{max}}\right) * \frac{1}{C_e} \quad (1)$$

where q_e is the amount of ions adsorbed in the equilibrium, K_L is the Langmuir constant and C_e represents the ion concentration in solution at equilibrium. It is possible to find an estimation of K_L and q_{max} from the plotting of $1/q_e$ vs. $1/C_e$ [26].

The Freundlich linearized equation is:

$$\log q_e = \log K_F + \frac{1}{n} \log C_e \quad (2)$$

where K_F is the model constant. By plotting $\log q_e$ vs. $\log C_e$ the n and K_F parameters can be defined. The n parameter indicates the magnitude of the adsorption driving force or the surface heterogeneity. The adsorption isotherm is linear when $n = 1$, favorable when $n < 1$, and unfavorable when $n > 1$.

2.5. Adsorption Kinetics

To the kinetics studies, adsorption tests were carried out with 25 mg L^{-1} nickel solutions with contact time with the biosorbent varying from 10 to 1440 min. After each evaluation time, the samples were filtered, and the adsorption rates were determined by spectrophotometry. The pseudo-first order, pseudo-second order, Elovich and intraparticle diffusion models were used to describe the kinetics.

The pseudo-first order equation (Equation (3)) was proposed by [26]. It is generally used in the form proposed by [27]:

$$\frac{q}{q_e} + \ln(q_e - q) = \ln(q_e) - k_1 t \quad (3)$$

where the constant k_1 is a function of the method. Plotting ln ($q_e - q$) vs. t provides a value of k_1 and q_e.

Pseudo-second order model (Equation (4)) assumes that the rate is second order with respect to the available surface sites. The equation according to [26] is:

$$\frac{t}{q} = \frac{1}{k_2 q_e^2} + \frac{t}{q_e} \quad (4)$$

where k_2 is the constant of pseudo-second order found by the plot of t/q vs. t.

The Elovich equation (Equation (5)) is usually applied to describe chemical adsorption processes and is appropriate for systems with heterogeneous surfaces. A simplified equation was presented by [28]:

$$q = \left(\frac{1}{b}\right) \ln(ab) + \left(\frac{1}{b}\right) \ln t \quad (5)$$

where a and b are constants estimated by the plot of q vs. ln t.

The intraparticle diffusion as a diffusion-controlled process [29] is represented by Equation (6):

$$q_t = k_{\text{int}} t^{\frac{1}{2}} + C \quad (6)$$

where k_{int} is the constant, a plot of q_t versus $t^{1/2}$ should be a straight line with a slope k_{int} and intercept °C.

3. Results

3.1. Materials Characterization

The BET analysis (Table 1) shows the specific surface area of the different materials which is similar for walnut shell, chestnut shell and burnt pine wood, between 3.97 and 4.85 m^2g^{-1}. For these three materials the pore size varies between 5.40 and 7.33 nm. For pine wood the specific surface area and the pore size are completely different, 1.74 m^2g^{-1} and 26.54 nm, respectively.

Table 1. BET analysis of the several materials.

Materials	BET Surface Area (m^2g^{-1})	Pore Volume ($cm^3\ g^{-1}$)	Pore Size (nm)
Walnut shell	4.855	1.195×10^{-3}	5.41
Chestnut shell	4.210	4.202×10^{-3}	7.33
Pine wood	1.738	4.920×10^{-4}	26.54
Burnt pine wood	3.968	3.388×10^{-3}	5.40

The XRD patterns (Figure 1 and Supplementary Figures S1–S4) do not show sharp diffraction patterns. Two broad diffraction bands at ca. 16° and 22° 2θ are observed and assigned to cellulose [30]. The diffractograms witness some polycrystalline domain, but the bands are quite broad. In the case of the burnt pine wood, it is completely amorphous (Figure S1).

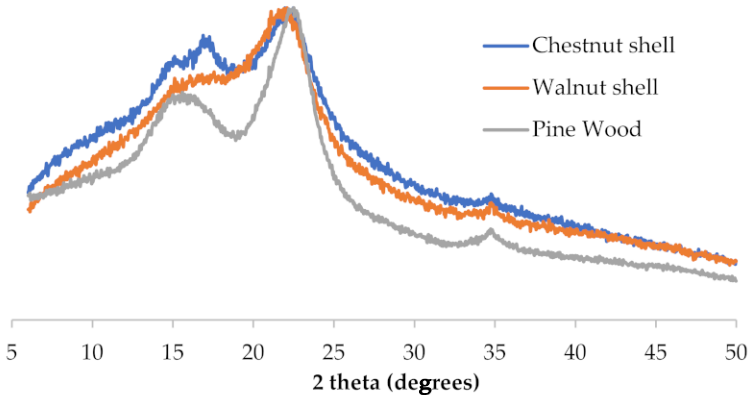

Figure 1. Powder X-ray diffraction of the different materials.

The results obtained from FTIR-ATR analysis are presented in the Figures 2–5, for walnut shell, chestnut shell, pine wood and burnt pine wood, respectively. Similar spectra are found for walnut shell and chestnut shell. Burnt pine wood presented a much different spectrum from the other materials. The FTIR spectra of walnut shells, chestnut shells and pine wood exhibit similar bands. The band at around 3430 cm^{-1} corresponds to O-H stretching vibration which is present either in polysaccharides and lignin. The main differences are that for pine wood the maximum is around 3330 cm^{-1} and for walnut and chestnut shells it is around 3320 cm^{-1}. The two bands at 2900–2800 cm^{-1} are composed by the overlapping of the stretch asymmetric vibrations of -CH_2- (generally around 2935–2915 cm^{-1}) and -CH_3 (2970–2950 cm^{-1}) and by the overlapping of stretch symmetric vibrations of -CH_2- (2865–2845 cm^{-1}) and -CH_3 (2880–2860 cm^{-1}) [31]. Generally, the asymmetric band presents higher absorptivity which in this case is only true for walnut shells and is somewhat true for pine wood. The region between 1750 and 1700 cm^{-1} is due to C=O linkage that exhibits strong absorption which can be at smaller or higher wavelength according to the functional group [32]. Walnut shells presented the highest absorption at these wavelengths. The band at around 1595 cm^{-1} has been attributed to vibrations in the aromatic ring of lignin plus C=O stretching. Aromatic rings are known to exhibit a band at approximately 1500 cm^{-1}, corresponding to benzene ring stretching vibrations.

This band was higher in the pine wood spectrum. The peak at around 1025–1035 cm^{-1} assigned to C-O-C deformation mostly present in carbohydrates was higher in the chestnut shells spectrum. The walnut shell spectrum after nickel adsorption was similar to the initial spectrum with the exception of the two bands at 2900–2800 cm^{-1} which decrease slightly, and the maximum seems to shift from asymmetric to symmetric vibrations and the peak at around 1730 cm^{-1} also decreases.

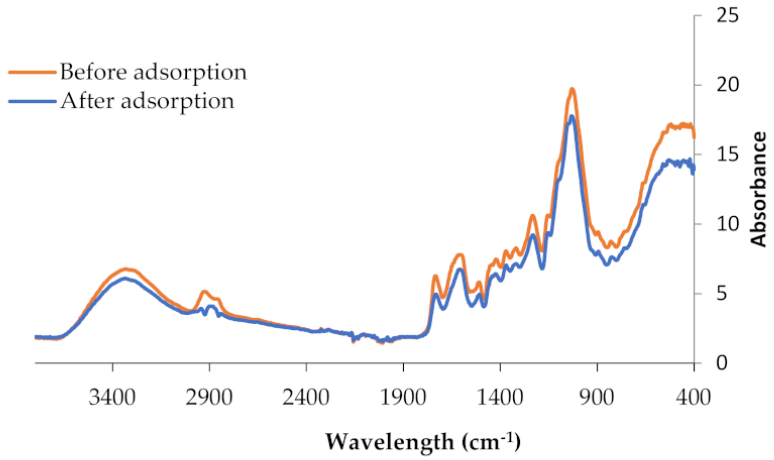

Figure 2. Characterization of walnut shell by FTIR-ATR analysis.

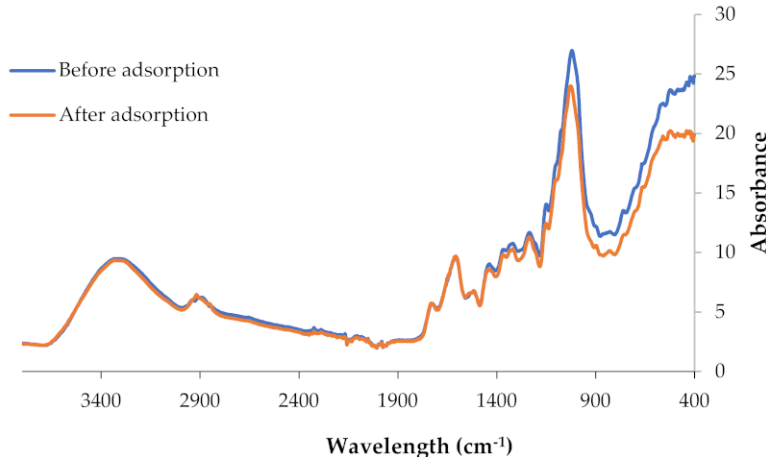

Figure 3. Characterization of chestnut shell by FTIR-ATR analysis.

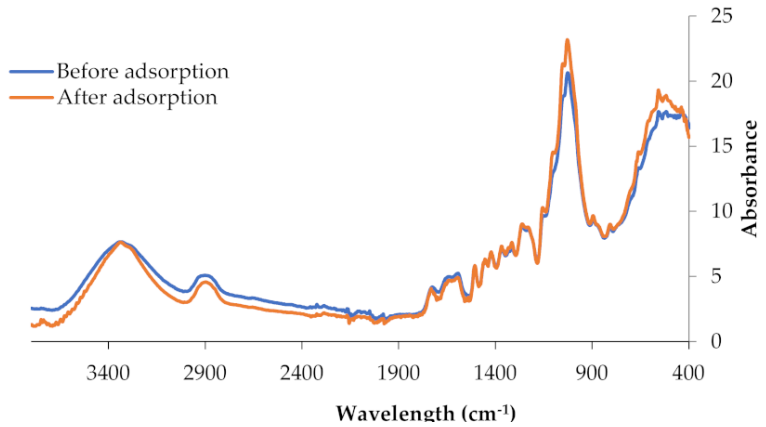

Figure 4. Characterization of pine wood by FTIR-ATR analysis.

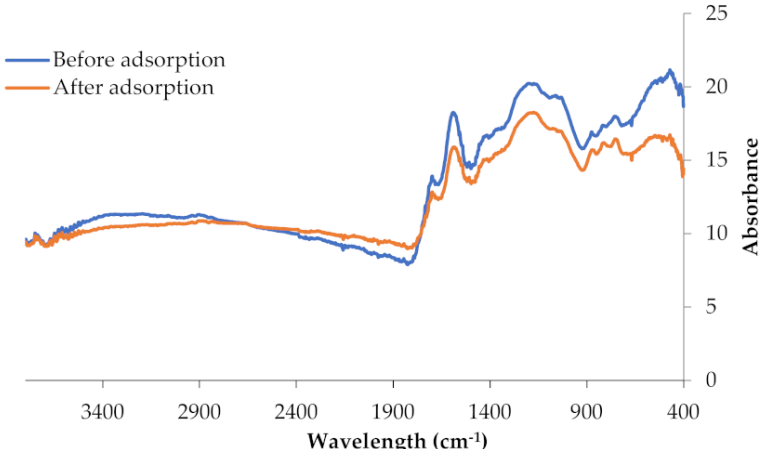

Figure 5. Characterization of burnt pine wood by FTIR-ATR analysis.

The chestnut shell spectrum after nickel adsorption was very similar to the initial spectrum except for the region between 900 and 1400 cm^{-1} where there seems to be a decrease in the 1144 cm^{-1} and 1010 cm^{-1} peak heights.

In relation to the pine wood spectrum after nickel adsorption the main differences are observed in the OH peak with an increase around 3315 cm^{-1} and in the peak's height at 1144 cm^{-1} and 1010 cm^{-1}, similar to chestnut shells.

The main difference is observed between the burnt pine wood spectrum and the other lignocellulosic materials. Burnt pine wood showed a lack of some functional groups compared to the other biosorbents. The OH stretching band around 3420 cm^{-1} is almost non-existent and the aliphatic CH band around 2900 cm^{-1} is very small compared to the other lignocellulosic materials. The C=O linkage band that generally exhibits strong absorptions in FTIR spectra between 1750 and 1700 cm^{-1} [31] could not be distinguished. The highest peak in the burnt pine wood spectrum is at 1580 cm^{-1} and it is much higher than for the other lignocellulosic materials. This band, generally at a slightly higher wavelength (1595 cm^{-1}) corresponds to vibrations in the aromatic ring of lignin plus C=O stretching [31]. The broad band between 1050 and 1300 cm^{-1} with the maximum around 1180 cm^{-1} is also attributed to lignin. The peak around 1025 cm^{-1} that is usually attributed to C-O-C deformation mostly from carbohydrates is very small compared to the other lignocellulosic materials. Comparing the spectrum between initial material and after nickel adsorption there is only a slight decrease around 1570 cm^{-1} and a slight increase around 1160 cm^{-1}.

The morphology of the different samples was studied using SEM images (Figures S5–S8). The different images do not show characteristic features; however, it is possible to see that there are no significative differences between the samples before and after reaction, for all the materials.

3.2. pH Optimization

The pH is important when working with heavy metal adsorption as it directly affects the amount of ions that can be removed from the aqueous solution. A pH variation can change the surface of the adsorbent, influencing electrostatic interactions with the solution [11]. The experimental results for the pH studies are presented in Figure 6.

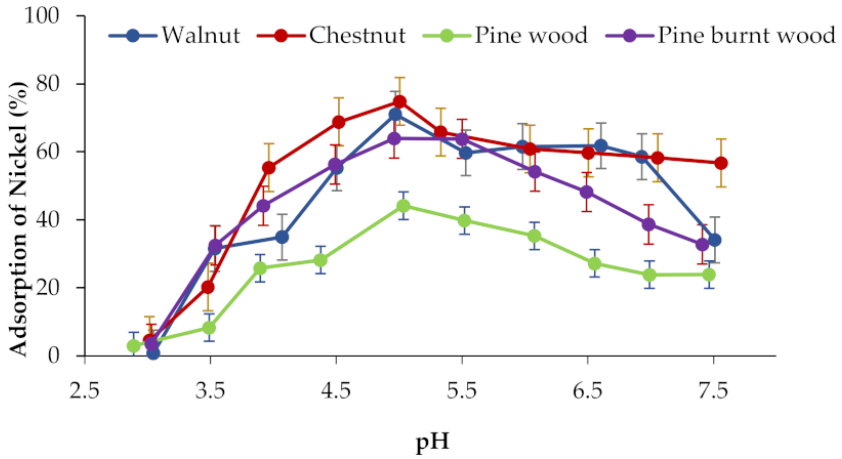

Figure 6. Adsorption rates under the range of pH tested with metal concentration of 200 mg L^{-1} and 100 mg of adsorbent.

The percentage of adsorption increased with pH until about pH 5.0 for all the materials studied. The best pH to remove nickel ions was around 5.0, where chestnut shell presented the highest adsorption percentage of almost 75% followed by walnut shell. Burnt pine wood showed slightly lower adsorption, while pine wood attained just over 40% adsorption. With the increase of pH after pH 5.0, all the percentages of adsorption decreased significantly.

3.3. Adsorption Isotherm

The adsorption isotherms were determined by testing the adsorption of increasingly higher amounts of nickel with the same amount of adsorbent at constant temperature. The most used isotherm models in these sorts of studies are Langmuir and Freundlich. The results found by plotting linearized Langmuir and Freundlich equilibrium isotherms are presented in Figures 7–9 and Table 2. In Table 2, determination coefficients (R^2) and the most important parameters for both types of isotherms are presented. The linearized forms were used due to their simplicity, although the non-linearized form was found to be a better way to obtain the isotherm parameters [33–35].

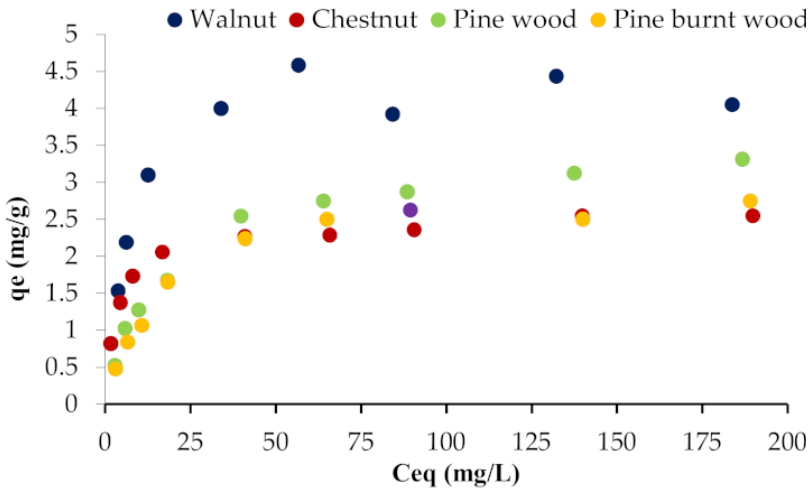

Figure 7. Adsorption isotherms of nickel for walnut shell, chestnut shell, pine wood and burnt pine wood with nickel concentrations from 5 to 200 mg L^{-1} and 100 mg of adsorbent.

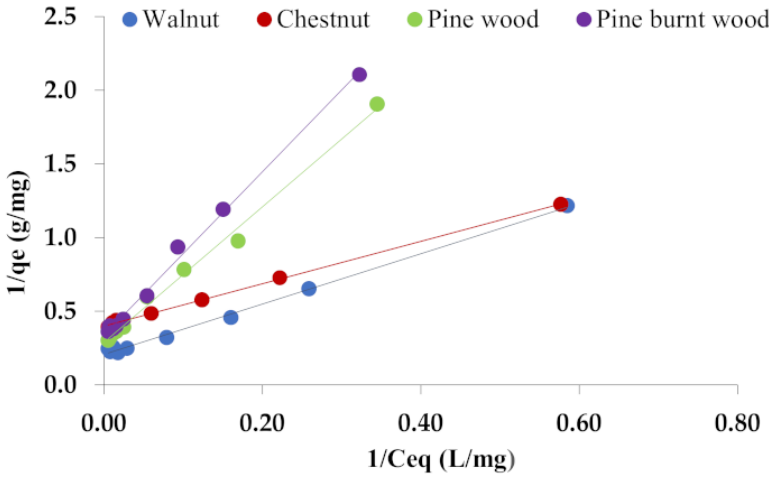

Figure 8. Langmuir isotherm model for nickel adsorption with nickel concentrations from 5 to 200 mg L^{-1} and 100 mg of adsorbent.

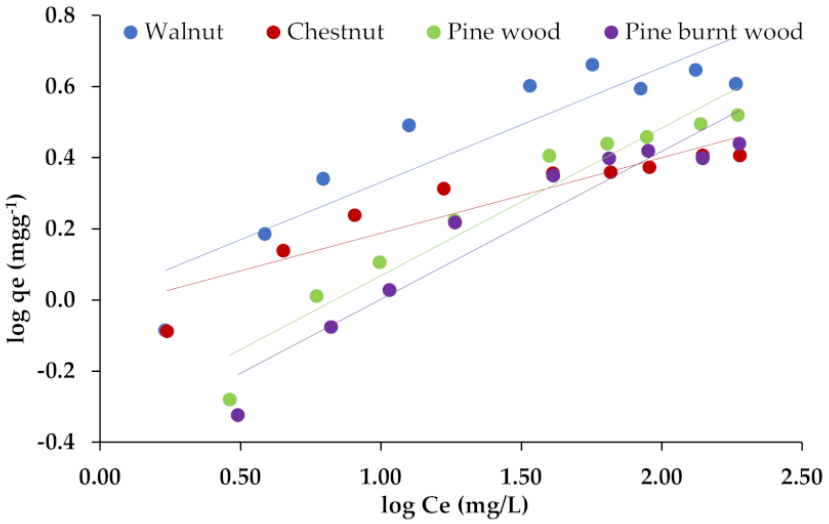

Figure 9. Freundlich isotherm model for nickel adsorption with nickel concentrations from 5 to 200 mg L^{-1} and 100 mg of adsorbent.

Table 2. Isotherm parameters of nickel adsorption onto the lignocellulosic materials.

	Langmuir			Freundlich		
	R^2	q_{max} (mg g^{-1})	K_L (L mg^{-1})	R^2	N	K_F (mg/g)/(mg/L)^n
Walnut shell	0.996	4.82	0.121	0.942	2.11	0.781
Chestnut shell	0.998	2.50	0.278	0.859	4.72	0.946
Pine wood	0.994	3.45	0.063	0.936	2.41	0.449
Burnt pine wood	0.996	2.97	0.061	0.911	2.41	0.386

3.4. Kinetics Studies

The study of adsorption kinetics allows us to perceive how fast the process takes place and can indicate its limiting factor. Adsorption kinetics can be represented by a graph of adsorption versus time (Figure 10). This graph forms the basis of kinetic studies, as its shape represents the intrinsic kinetics of the process, which depends on factors such as the type of adsorbent and adsorbate, temperature and pH [36]. The steps for determining the adsorption rate include the diffusion process, chemical reactions and particle diffusion [37]. The most applied models in the study of adsorption kinetics are pseudo-first order and

pseudo-second order [36]. In this case study, the Elovich and intraparticle diffusion models were also tested.

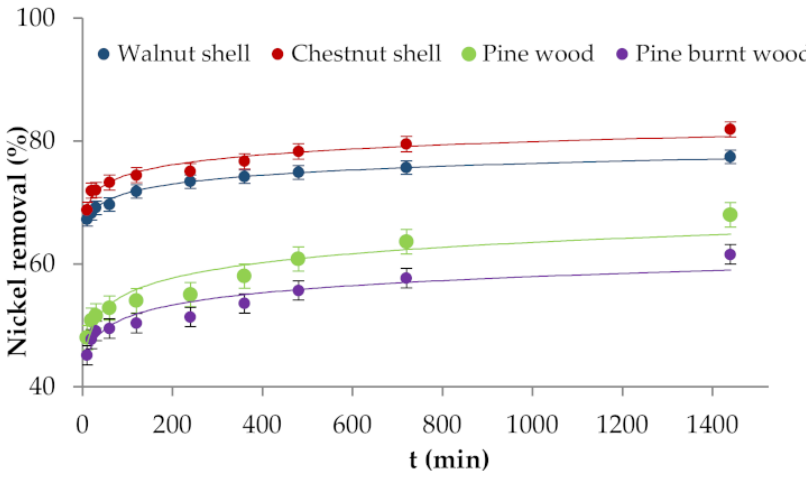

Figure 10. Adsorption efficiency versus time, from 10 to 1440 min by the different adsorbent materials using 25 mg L^{-1} nickel solutions and 100 mg of adsorbent.

The most frequently used kinetics models are pseudo-first order (PFO) and pseudo-second order (PSO) equations [36] since they seem to work very well with the adsorption by lignocellulosic materials. Additionally, Elovich and intraparticle diffusion models were also tested. The results found by plotting pseudo-first order and pseudo-second order models are presented in Table 3 and results for Elovich and intraparticle diffusion models are presented in Table 4.

Table 3. Parameters for the kinetic sorption data using pseudo-first order and pseudo-second order kinetic models.

Biosorbent	Pseudo-First Order Model				Pseudo-Second Order Model				
	k_1 (min^{-1})	q_e Calc ($mg \cdot g^{-1}$)	q_e Exp ($mg \cdot g^{-1}$)	R^2	k_2 ($g \cdot mg \cdot min^{-1}$)	h ($mg \cdot g \cdot min^{-1}$)	q_e Calc ($mg \cdot g^{-1}$)	q_e Exp ($mg \cdot g^{-1}$)	R^2
Walnut shell	2.50×10^{-3}	0.546	4.84	0.956	2.46×10^{-2}	0.575	4.84	4.84	1.000
Chestnut shell	2.20×10^{-3}	0.675	5.12	0.966	2.13×10^{-2}	0.527	4.98	5.12	1.000
Pine wood	1.90×10^{-3}	1.156	4.25	0.977	1.07×10^{-2}	0.169	3.98	4.25	0.998
Burnt pine wood	1.80×10^{-3}	0.907	3.85	0.971	1.47×10^{-2}	0.191	3.61	3.85	0.999

Table 4. Parameters for the kinetic data using Elovich and intraparticle diffusion models.

Biosorbent	Elovich Model			Intraparticle Diffusion Model		
	A ($mg \cdot g^{-1} \cdot min^{-1}$)	B ($g \cdot mg^{-1}$)	R^2	C	Kdif ($mg/g \cdot min^{1/2}$)	R^2
Walnut shell	9.94×10^{10}	6.84	0.956	4.23	0.019	0.924
Chestnut shell	1.05×10^{12}	7.67	0.990	4.37	0.021	0.942
Pine wood	1.00×10^{4}	4.44	0.905	2.99	0.035	0.978
Burnt pine wood	1.09×10^{5}	5.59	0.908	2.84	0.027	0.970

The adsorption rate was higher in the beginning of the adsorption process, decreasing afterwards. This means that when all the adsorption sites are free, the adsorption process is faster but when the adsorption sites start to be occupied, the adsorption rate decreases. Nevertheless, the highest adsorption was reached for 1440 min. It was also observed that the removal rate promoted by chestnut shell and walnut shell was higher than the rate promoted by pine wood and burnt pine wood.

4. Discussion

The main advantage of using waste lignocellulosic materials like the ones tested here is that they do not need to be reused since they are very cheap materials. Any process to reuse these materials would be far more expensive than using new ones. The specific surface area determined by BET (Table 1) for the different materials was very similar for walnut shell, chestnut shell and burnt pine wood, being around 4 m^2g^{-1}, higher than the 1.74 m^2g^{-1} found in pine wood. The partial burning of pine wood increased the specific surface area to more than double, which showed some effect on the adsorption phenomenon. The specific area of burnt pine wood is similar to that of biochars prepared from rice straw at 400 °C (4.4 m^2g^{-1}) but lower than the ones obtained at 700 °C (116.2 m^2g^{-1}) [38]. The specific area of 3.97 m^2g^{-1} was obtained for waste-apricot-activated carbon prepared by chemical activation at lower temperature (400 °C) which is similar to the materials tested here. Of course, when comparing the same material chemically activated at 900 °C with specific area of 1214 m^2g^{-1} the values are much lower [39]. The lower adsorption area (Table 1) of pine wood might be one of the main reasons for the lower adsorption observed for pine wood in Figure 6 compared to the remaining materials such as walnut and chestnut shells. On the other hand, the pore size varied between 5.40 and 7.33 nm for the remaining materials and was higher at 26.54 nm for pine wood. Higher-size micropores generally lead to a transition towards a surface or multilayer adsorption mechanism [40,41]. The physical adsorption mechanism in small micropores is mainly pore filling because the overlapping of pore wall potentials results in stronger binding of the adsorbate, or enhanced adsorption.

The diffractograms witness some polycrystalline domain for most of the materials with quite broad bands. In the case of the burnt pine wood, it was completely amorphous (Figure S1). The metal adsorption on lignocellulosic materials is mainly due to the high diversity and number of functional groups. FTIR-ATR tests were made to characterize the initial materials' functional groups and to determine possible changes in the spectra after nickel adsorption. All lignocellulosic materials showed high diversity of functional groups except for burnt pine wood which might justify the lower adsorption presented in Figure 7 by burnt pine wood. This functional group diversity allows, in accordance with Asberry et al. [21], positively charged heavy metal ions to bind with these groups, under suitable pH conditions which have been found in Figure 6 via charge interaction, to be adsorbed onto the biosorbent particles. In accordance with Kulkarni et al. [42], many functional groups were affected by the adsorption of nickel on *Bacillus laterosporus*. The reported mechanisms were ion exchange, adsorption and complexation.

The best adsorption rates with pH (Figure 6) were obtained by chestnut shell with adsorption around 75%, followed by walnut shell attaining an adsorption of 71%, pine wood and burnt pine wood that presented ca. 44% and ca. 64%, respectively. Although walnut shell had the highest surface area, at pH 5 the adsorption is slightly higher for chestnut shell. Nevertheless, the difference is not significative, and adsorption is not only dependent on the specific surface area but also on the pore size and pore volume and on the chemical composition of the material. The higher pore volume and pore size obtained for chestnut shell in relation to walnut shell might explain this difference. Similarly to other studies, optimal conditions were demonstrated to be attained at pH 5.0, for example for activated carbon prepared from almond husk [43]. Nevertheless, pH 6.0 was found to be the optimal pH to remove nickel by rice husk ash [9]. Sugarcane bagasse was analyzed as an adsorbent, and the maximum removal rate was observed at pH 6.5 [10]. Once the pH basic is near, nickel precipitation occurs [36], which also depends on the concentration of metal in the solution. This might be the reason for the decreased percentage of adsorption after pH 5.0. A similar increase in adsorption until pH 5 was reported previously [2,44]. These authors stated that metal adsorption is mostly based on an ion exchange mechanism between metal ions and existing counter-ions on negatively charged ionic groups and that metal ions must compete with protons for the binding sites. Therefore, higher pH will mean lower competition and higher adsorption.

The mechanisms that occur during the retention of ions in a biosorbent are directly related to the functional groups present in the material. These groups are normally present in structures in the cell wall, which include cellulose organized in microfibers, surrounded by hemicelluloses, lignin, pectin and small quantities of proteins. This way, the retention of metal ions by the material surface also depends on its chemical composition, which explains the variability found for each material. Nevertheless, since only the initial pH of the solution is measured, the final pH of the water with the adsorbent might also contribute to the differences between materials.

Figure 7 presents the adsorption isotherms of nickel for walnut shell, chestnut shell, pine wood and burnt pine wood. Results show that equilibrium is reached for around 100 mg/L for most of the materials. Walnut shell adsorption was not very consistent for concentrations higher than 100 mg/L but this is probably due to the major errors obtained when determining higher concentrations in atomic adsorption. The data suggest that equilibrium was reached earlier in chestnut shell which can be due to the combination of higher pore volume and the second highest pore size, since this is in accordance with Pelekani and Snoeyink [40], where higher pore size and pore volume adsorption equilibrium is achieved earlier. The Langmuir model (Figure 8) assumes that when adsorption occurs in a monolayer surface, with a finite number of active sites and homogeneous energy of adsorption, no additional adsorption can occur at the same site [11]. The theory is based on the fact that adsorption occurs at uniform sites [45], and takes place without interaction between the adsorbed molecules [37]. Each active site is equal, with the capability to attach particles independent of other active sites being filled or not [11].

On the other hand, Freundlich isotherm (Table 2) is derived by assuming a heterogeneous surface with a non-uniform distribution of heat of adsorption over the surface [24]. The heterogeneity of the adsorbent surface affects adsorption equilibrium and kinetics [46]. Heterogeneous surfaces include more than one type of adsorption site, and each type has a distinct heat of sorption. It is a model that is suitable for multilayer adsorption, for adsorbents with a heterogeneous surface and a uniform distribution of adsorption heat [11]. The model considers that metal ions are infinitely accumulated on the surface of the adsorbent [45]. Thus, the adsorptive capacity is related to the concentration of metal ions in equilibrium in the solution.

The experimental results showed that the Langmuir model fitted the sorption processes best because it presented higher R^2 for all biosorbents tested, with values ranging between 0.994 for pine wood and 0.998 for chestnut shell. As found in this study, the sorption promoted by activated carbon prepared from almond husk was better described by the Langmuir isotherm with R^2 = 0.983 and 0.995 [43]. Similarly, the nickel sorption by protonated rice bran fitted well with the Langmuir isotherm model with R^2 about 0.941 [5]. Even though the Langmuir model presented the best results, the Freundlich model also predicted the adsorption process well.

The $q_{máx}$, which corresponds to the saturation capacity of the adsorbent material estimated by Langmuir plotting was around 2.50 mg g^{-1} (chestnut) to 4.82 mg g^{-1} (walnut), lower than the values obtained by [5,47], around 50 mg g^{-1} for *Punica granatum* peel and 44.90 mg g^{-1} for protonated rice bran, respectively. Nevertheless, the values are higher than the ones reported for the adsorption of nickel ions onto coal fly ash with just 0.30 mg g^{-1} [30]. The *n* value from Freundlich isotherm varied from 2.41 to 4.72 which shows the good ability of these lignocellulosic adsorption materials since a good adsorption has been reported to be with *n* values ranging from 1 to 10 as reported before [17,47,48]; a similar result was found by [5] with *n* around 2.31 or by [30] with 2.57 for *n*.

Adsorption presented in Figure 10 shows different nickel percentage removal than Figure 6 since pH optimization was made with 200 mg/L of nickel solutions while adsorption kinetics was made with 25 mg/L. This is possibly due to the major importance of the specific area rather than the existence of functional groups at higher nickel concentration. The PFO presumes that the adsorption rate is proportional to the difference between the equilibrium adsorption capacity and the quantity of adsorption. The PSO assumes that

the adsorption process includes membrane diffusion and surface adsorption and can also describe the mechanism in a more realistic way [46]. In relation to adsorption kinetics, the pseudo-second order reaction was the model that best represented the sorption process for all materials under evaluation. The R^2 values were between 0.998 for pine wood and 1.00 for walnut shell and chestnut shell. However, PFO showed a correlation greater than 0.90, but with lower values than those indicated by PSO. PFO was shown to be valid to describe the process only at the initial stage of adsorption [46]. There are two different phases, one until about 100 min with a higher slope and another one after that. Similarly, the adsorption of Ni by Bael tree leaf powder [49], protonated rice bran [5] and mesoporous rice husk ash [9] obeys the pseudo-second order kinetics with correlation values around 0.988, 1.00 and 0.999, respectively. A preference for PSO over PFO has generally been found in studies where a comparison of the two equations is made [29].

Elovich equation is known to describe chemisorption well. Many works assumed that the equation had a relation with strong heterogeneity at the adsorbent surface [46]. Elovich equation is known to describe chemisorption well as stated before, so the occurrence of chemical reactions between the surface and the adsorbate cannot be discharged specially for the shells used in this study. Nevertheless, the differences between the R^2 of both models are small and therefore no conclusions can be drawn about their importance in practical adsorption filters. Intraparticle diffusion is characterized by the transport of the adsorbate in solution to the active sites of the adsorbent by mass transfer. In some cases, the intraparticle diffusion may not be involved in the whole adsorption process [11] but rather explains only part of it, which seems to be happening here in nickel adsorption by lignocellulosic materials.

The development of good adsorption includes three or four main steps: first, the external diffusion, which is the transportation of adsorbate to the external surface of adsorbent which, according to some authors, is divided into transport to the boundary layer and diffusion through the boundary layer to the external surface of the particle [50]; then, the intraparticle diffusion, which is the transference from the external surface into the pores; finally, the surface reaction, which is the attachment of adsorbate in the surface of the material [27,46,50,51]. The biosorption of cadmium and nickel ions using *Spirulina platensis* was reported to be well explained by the intraparticle diffusion model [44], which these authors stated is composed of more than one sorption process.

Physisorption is a consequence of attractive forces between adsorbate and sorbent, whereas chemisorption provides a stronger connection as it involves the transfer or sharing of electrons between compounds. The monolayer capacity is the capacity to accommodate a single layer of adsorbed species on the adsorbent surface. Often, when adsorptive concentration is elevated, because of intermolecular attraction, additional layers stack onto the first monolayer, creating multilayer adsorption [27].

According to the results found by plotting Elovich and intraparticle diffusion models, it was possible to state that the Elovich model described the kinetics well for walnut and chestnut shells, with correlation values of 0.956 for walnut and 0.990 for chestnut. Otherwise, the adsorption processes for pine wood and burnt pine wood were best described by the intraparticle diffusion model, with R^2 = 0.970 for burnt pine wood and 0.978 for pine wood. The differences are, however, small and therefore none of the models can be excluded. All sorption kinetic models presented R^2 higher than 0.90, which means that more than one sorption process may take place in the nickel adsorption system by the biosorbents tested.

SEM testing showed characteristic features; however, there were no significative differences between the samples before and after reaction for all the materials. Several authors confirmed the metal intake by SEM; Abdolali et al. [52] stated that SEM analysis showed morphology changes of unloaded and loaded tea waste–mandarin peels–maple leaves and that after nickel adsorption, the surface became smoother, with less porosity, which was associated with probable metal entrapping on biosorbent. In accordance with Lee et al. [53], the rough and porous surface *Cymbopogon citratus* (lemon grass) particles

tested as biosorbent may provide possible sorption sites for the uptake of Ni^{2+}. Bean- and lump-like deposits were observed on the surface of the biosorbent following adsorption of Ni(II) [20].

5. Conclusions

The material characterization showed that the materials have similar specific surface areas between 3.97 and 4.85 m^2g^{-1} except pine wood with 1.74 m^2g^{-1} that had higher pore size of 26.54 nm compared to the remaining materials (5.40–7.33 nm). The diffractograms analysis showed that all the lignocellulosic materials presented some crystalline domains except for burnt pine wood, which was completely amorphous. All materials showed similar lignocellulosic characteristic FTIR bands with the main difference observed in the burnt pine wood spectrum that had a lack of some functional groups compared to the other biosorbents.

The best pH to remove nickel was found to be around 5.0. At this pH the adsorption was higher for chestnut shells, walnut shells, burnt pine wood and pine wood, respectively.

The Langmuir model fitted the sorption process best. This means that the sorption mostly takes place at specific homogeneous sites of the biosorbent. Nevertheless, since Freundlich isotherm also gives good results, we cannot discard the possibility of adsorption happening in heterogeneous sites.

The kinetics was well described by PFO and PSO, but pseudo-second order presented higher R^2 to all biosorbents tested.

The Elovich and intraparticle diffusion models presented R^2 greater than 0.90, which means that the sorption process may occur in more than one way. The Elovich equation is known to describe chemisorption well; therefore, the occurrence of chemical reactions between the surface and the adsorbate cannot be discharged. The intraparticle diffusion model may not be involved in the whole adsorption process but might explain some part of nickel adsorption onto lignocellulosic materials.

Finally, the results show that walnut shell, chestnut shell, pine wood and burnt pine wood can be applied as adsorbent materials and have the capability to remove nickel from aqueous solutions.

Supplementary Materials: The following are available online at https://www.mdpi.com/article/10.3390/app12020933/s1, Figure S1: Powder X-ray diffraction of all the materials, Figure S2: Powder X-ray diffraction of wood before and after reaction, Figure S3: Powder X-ray diffraction of chestnut shell before and after reaction, Figure S4: Powder X-ray diffraction of walnut shell before and after reaction, Figure S5: SEM images from wood (a) before, (b) after 10 min of reaction and (c) after 25 min of reaction, Figure S6: SEM images from chestnut shell (a) before, (b) after 10 min of reaction and (c) after 25 min of reaction, Figure S7: SEM images from walnut shell (a) before, (b) after 10 min of reaction and (c) after 25 min of reaction, Figure S8: SEM images from burnt wood (a) before, (b) after 10 min of reaction and (c) after 25 min of reaction.

Author Contributions: Conceptualization by L.C.-L.; investigation by M.M.; formal analysis by M.M. and I.S.-V., helped by L.C.-L.; writing, review and editing were performed by all authors; and funding acquisition by B.E. and L.C.-L. All authors have read and agreed to the published version of the manuscript.

Funding: National Funds through the FCT—Foundation for Science and Technology, I.P., within the scope of the project Ref[a] UIDB/00681/2020. I.C.M.S.S.-V. (Ref. 197_97_ARH-2018) was financed by the National Funds (OE), through FCT, I.P., under the framework contract provided for in paragraphs 4, 5 and 6 of Article 23 of Decree-Law 57/2016 of August 29, as changed by Law No. 57/2017 of July 19.

Institutional Review Board Statement: Not applicable.

Informed Consent Statement: Not applicable.

Data Availability Statement: Not applicable.

Acknowledgments: Furthermore, we would like to thank the CERNAS Research Centre and the Polytechnic Institute of Viseu for their support.

Conflicts of Interest: The authors declare no conflict of interest. The funders had no role in the design of the study; in the collection, analyses, or interpretation of data; in the writing of the manuscript, or in the decision to publish the results.

References

1. Furlan, F.L.; Consolin, N.; Consolin, M.F.B.; Gonçalves, M.S.; Valderrama, P.; Genena, A.K. Use of agricultural and agroindustrial residues as alternative adsorbents of manganese and iron in aqueous solution. *Rev. Ambiente Água* **2018**, *13*, 1–13. [CrossRef]
2. Gürel, L. Applications of the Biosorption Process for Nickel Removal from Aqueous Solutions—A Review. *Chem. Eng. Commun.* **2017**, *204*, 711–722. [CrossRef]
3. Malamis, S.; Katsou, E. A review on zinc and nickel adsorption on natural and modified zeolite, bentonite and vermiculite: Examination of process parameters, kinetics and isotherms. *J. Hazard. Mater.* **2013**, *252–253*, 428–461. [CrossRef] [PubMed]
4. Decreto-Lei n.º 236/98. de 1 de Agosto. Série I-A de 1998-08-01. 1 August 1998, pp. 3676–3722. Available online: https://dre.pt/dre/detalhe/decreto-lei/236-1998-430457 (accessed on 10 December 2021).
5. Zafar, M.N.; Nadeem, R.; Hanif, M.A. Biosorption of nickel from protonated rice bran. *J. Hazard. Mater.* **2007**, *143*, 478–485. [CrossRef] [PubMed]
6. Carrapatoso, I.; Loureiro, G.; Loureiro, C.; Faria, E.; Todo-Bom, A.; Chieira, C. Dermatite endógena induzida pela ingestão de níquel: A propósito de dois casos clínicos. Nickel Induc. Endog. Dermat. Two Cases Report. *Revist. Portuguesa de Imunoalergologia.* **2004**, *XII*, 261–270.
7. Duarte, R.P.S.; Pasqual, A. Avaliação do cádmio (Cd), chumbo (Pb), níquel (Ni) e zinco (Zn) em solos, plantas e cabelos humanos. *Energ. na Agric.* **2000**, *15*, 46–58.
8. Raval, N.P.; Shah, P.U.; Shah, N.K. Adsorptive removal of nickel(II) ions from aqueous environment: A review. *J. Environ. Manag.* **2016**, *179*, 1–20. [CrossRef] [PubMed]
9. Srivastava, V.C.; Mall, I.D.; Mishra, I.M. Characterization of mesoporous rice husk ash (RHA) and adsorption kinetics of metal ions from aqueous solution onto RHA. *J. Hazard. Mater.* **2006**, *134*, 257–267. [CrossRef]
10. Krishna, V.D.; Wu, K.; Su, D.; Cheeran, M.C.J.; Wang, J.-P.; Perez, A. Nanotechnology: Review of concepts and potential application of sensing platforms in food safety. *Food Microbiol.* **2018**, *75*, 47–54. [CrossRef]
11. Ali, R.M.; Hamad, H.A.; Hussein, M.M.; Malash, G.F. Potential of using green adsorbent of heavy metal removal from aqueous solutions: Adsorption kinetics, isotherm, thermodynamic, mechanism and economic analysis. *Ecol. Eng.* **2016**, *91*, 317–332. [CrossRef]
12. Chen, D.; Wang, L.; Ma, Y.; Yang, W. Super-adsorbent material based on functional polymer particles with a multilevel porous structure. *NPG Asia Mater.* **2016**, *8*, e301. [CrossRef]
13. Naseer, A.; Jamshaid, A.; Hamid, A.; Muhammad, N.; Ghauri, M.; Iqbal, J.; Rafiq, S.; Khuram, S.; Shah, N.S. Lignin and Lignin Based Materials for the Removal of Heavy Metals from Waste Water-An Overview. *Z. Für Phys. Chem.* **2019**, *233*, 315–345. [CrossRef]
14. Rajeshwarisivaraj; Sivakumar, S.; Senthilkumar, P.; Subburam, V. Carbon from Cassava peel, an agricultural waste, as an adsorbent in the removal of dyes and metal ions from aqueous solution. *Bioresour. Technol.* **2001**, *80*, 233–235. [CrossRef]
15. Sathishkumar, P.; Arulkumar, M.; Palvannan, T. Utilization of agro-industrial waste Jatropha curcas pods as an activated carbon for the adsorption of reactive dye Remazol Brilliant Blue R (RBBR). *J. Clean. Prod.* **2012**, *22*, 67–75. [CrossRef]
16. Junior, A.C.G.; Strey, L.; Lindino, C.A.; Nacke, H.; Schwantes, D.; Seidel, E.P. Applicability of the Pinus bark (*Pinus elliottii*) for the adsorption of toxic heavy metals from aqueous solutions. *Acta Sci. Technol.* **2012**, *34*, 79–87. [CrossRef]
17. Esteves, B.; Cruz-Lopes, L.; Figueirinha, A.; de Lemos, L.T.; Ferreira, J.; Pereira, H.; Domingos, I. Heat-treated wood as chromium adsorption material. *Eur. J. Wood Wood Prod.* **2017**, *75*, 903–909. [CrossRef]
18. Doke, K.M.; Khan, E.M. Equilibrium, kinetic and diffusion mechanism of Cr (VI) adsorption onto activated carbon derived from wood apple shell. *Arab. J. Chem.* **2017**, *10*, S252–S260. [CrossRef]
19. Bhatnagar, A.; Sillanpää, M. Utilization of agro-industrial and municipal waste materials as potential adsorbents for water treatment—A review. *Chem. Eng. J.* **2010**, *157*, 277–296. [CrossRef]
20. Kamari, A.; Yusoff, S.N.M.; Abdullah, F.; Putra, W.P. Biosorptive removal of Cu (II), Ni (II) and Pb (II) ions from aqueous solutions using coconut dregs residue: Adsorption and characterisation studies. *J. Environ. Chem. Eng.* **2014**, *2*, 1912–1919. [CrossRef]
21. Asberry, H.B.; Kuo, C.-Y.; Gung, C.-H.; Conte, E.D.; Suen, S.-Y. Characterization of water bamboo husk biosorbents and their application in heavy metal ion trapping. *Microchem. J.* **2014**, *113*, 59–63. [CrossRef]
22. Özçimen, D.; Ersoy-Meriçboyu, A. Removal of copper from aqueous solutions by adsorption onto chestnut shell and grapeseed activated carbons. *J. Hazard. Mater.* **2009**, *168*, 1118–1125. [CrossRef]
23. Yang, J.-K.; Kim, H.-J.; Lee, W.-H. Changes of specific surface area of the steam exploded wood. *J. Korean Wood Sci. Technol.* **1995**, *23*, 54–60.
24. Aygün, A.; Yenisoy-Karakaş, S.; Duman, I. Production of granular activated carbon from fruit stones and nutshells and evaluation of their physical, chemical and adsorption properties. *Microporous Mesoporous Mater.* **2003**, *66*, 189–195. [CrossRef]

25. Velić, N.; Stjepanović, M.; Begović, L.; Habuda-Stanić, M.; Velić, D.; Jakovljević, T. Valorisation of waste wood biomass as biosorbent for the removal of synthetic dye methylene blue from aqueous solutions. *South-East Eur. For.* **2018**, *9*, 115–122. [CrossRef]
26. Lagergren, S.K. About the theory of so-called adsorption of soluble substances. *Sven Vetenskapsakad Handingarl* **1898**, *24*, 1–39.
27. Ho, Y.S.; McKay, G. Pseudo-second order model for sorption processes. *Process Biochem.* **1999**, *34*, 451–465. [CrossRef]
28. Wu, F.-C.; Tseng, R.-L.; Juang, R.-S. Characteristics of Elovich equation used for the analysis of adsorption kinetics in dye-chitosan systems. *Chem. Eng. J.* **2009**, *150*, 366–373. [CrossRef]
29. Simonin, J.-P. On the comparison of pseudo-first order and pseudo-second order rate laws in the modeling of adsorption kinetics. *Chem. Eng. J.* **2016**, *300*, 254–263. [CrossRef]
30. Agarwal, U.P.; Ralph, S.A.; Baez, C.; Reiner, R.S.; Verrill, S.P. Effect of sample moisture content on XRD-estimated cellulose crystallinity index and crystallite size. *Cellulose* **2017**, *24*, 1971–1984. [CrossRef]
31. Esteves, B.; Velez Marques, A.; Domingos, I.; Pereira, H. Chemical changes of heat treated pine and eucalypt wood monitored by FTIR. *Maderas Cienc. Tecnol.* **2013**, *15*, 245–258. [CrossRef]
32. Rodrigues, J.; Faix, O.; Pereira, H. Determination of lignin content of Eucalyptus globulus wood using FTIR spectroscopy. *Holzforschung* **1998**, *52*, 46–50. [CrossRef]
33. Kumar, K.V.; Sivanesan, S. Prediction of optimum sorption isotherm: Comparison of linear and non-linear method. *J. Hazard. Mater.* **2005**, *126*, 198–201. [CrossRef] [PubMed]
34. Kumar, K.V.; Porkodi, K.; Rocha, F. Comparison of various error functions in predicting the optimum isotherm by linear and non-linear regression analysis for the sorption of basic red 9 by activated carbon. *J. Hazard. Mater.* **2008**, *150*, 158–165. [CrossRef]
35. Subramanyam, B.; Das, A. Linearized and non-linearized isotherm models comparative study on adsorption of aqueous phenol solution in soil. *Int. J. Environ. Sci. Technol.* **2009**, *6*, 633–640. [CrossRef]
36. Tan, K.L.; Hameed, B.H. Insight into the adsorption kinetics models for the removal of contaminants from aqueous solutions. *J. Taiwan Inst. Chem. Eng.* **2017**, *74*, 25–48. [CrossRef]
37. Badawi, M.A.; Negm, N.A.; Abou Kana, M.T.H.; Hefni, H.H.; Abdel Moneem, M.M. Adsorption of aluminum and lead from wastewater by chitosan-tannic acid modified biopolymers: Isotherms, kinetics, thermodynamics and process mechanism. *Int. J. Biol. Macromol.* **2017**, *99*, 465–476. [CrossRef] [PubMed]
38. Deng, Y.; Huang, S.; Dong, C.; Meng, Z.; Wang, X. Competitive adsorption behaviour and mechanisms of cadmium, nickel and ammonium from aqueous solution by fresh and ageing rice straw biochars. *Bioresour. Technol.* **2020**, *303*, 122853. [CrossRef] [PubMed]
39. Erdoğan, S.; Önal, Y.; Akmil-Başar, C.; Bilmez-Erdemoğlu, S.; Sarıcı-Özdemir, Ç.; Köseoğlu, E.; Icduygu, G. Optimization of nickel adsorption from aqueous solution by using activated carbon prepared from waste apricot by chemical activation. *Appl. Surf. Sci.* **2005**, *252*, 1324–1331. [CrossRef]
40. Pelekani, C.; Snoeyink, V.L. Competitive adsorption between atrazine and methylene blue on activated carbon: The importance of pore size distribution. *Carbon* **2000**, *38*, 1423–1436. [CrossRef]
41. Mamchenko, A.V.; Yakimova, T.I.; Koganovskii, A.M. The mechanism of the filling of the micropores in activated charcoals during the adsorption of organic substances dissolved in water. *Russ. J. Phys. Chem.* **1982**, *56*, 741.
42. Kulkarni, R.M.; Shetty, K.V.; Srinikethan, G. Cadmium (II) and nickel (II) biosorption by Bacillus laterosporus (MTCC 1628). *J. Taiwan Inst. Chem. Eng.* **2014**, *45*, 1628–1635. [CrossRef]
43. Hasar, H. Adsorption of nickel(II) from aqueous solution onto activated carbon prepared from almond husk. *J. Hazard. Mater.* **2003**, *97*, 49–57. [CrossRef]
44. Çelekli, A.; Bozkurt, H. Bio-sorption of cadmium and nickel ions using Spirulina platensis: Kinetic and equilibrium studies. *Desalination* **2011**, *275*, 141–147. [CrossRef]
45. Moreira, D.A.; de Souza, J.A.R.; Silva, É.L.; Gonçalves, J.M.; Rezende, D.C.V.; Oliveira, W.M.; Ribeiro, W.A.S.; Rezende, J.G.F. Biossorção de metais pesados pela casca de ovo de galinhas poedeiras. *Rev. Ibero-Am. Ciênc. Ambient.* **2018**, *9*, 289–295. [CrossRef]
46. Wang, X.; Jiang, C.; Hou, B.; Wang, Y.; Hao, C.; Wu, J. Carbon composite lignin-based adsorbents for the adsorption of dyes. *Chemosphere* **2018**, *206*, 587–596. [CrossRef]
47. Delle Site, A. Factors Affecting Sorption of Organic Compounds in Natural Sorbent/Water Systems and Sorption Coefficients for Selected Pollutants. A Review. *J. Phys. Chem. Ref. Data* **2001**, *30*, 187–439. [CrossRef]
48. Febrianto, J.; Kosasih, A.N.; Sunarso, J.; Ju, Y.-H.; Indraswati, N.; Ismadji, S. Equilibrium and kinetic studies in adsorption of heavy metals using biosorbent: A summary of recent studies. *J. Hazard. Mater.* **2009**, *162*, 616–645. [CrossRef] [PubMed]
49. Kumar, P.S.; Ramalingam, S.; Kirupha, S.D.; Murugesan, A.; Vidhyadevi, T.; Sivanesan, S. Adsorption behavior of nickel(II) onto cashew nut shell: Equilibrium, thermodynamics, kinetics, mechanism and process design. *Chem. Eng. J.* **2011**, *167*, 122–131. [CrossRef]
50. Usman, M.; Zarebanadkouki, M.; Waseem, M.; Katsoyiannis, I.A.; Ernst, M. Mathematical modeling of arsenic (V) adsorption onto iron oxyhydroxides in an adsorption-submerged membrane hybrid system. *J. Hazard. Mater.* **2020**, *400*, 123221. [CrossRef] [PubMed]
51. Martínez-Cabanas, M.; López-García, M.; Barriada, J.L.; Herrero, R.; de Vicente, M.E.S. Green synthesis of iron oxide nanoparticles. Development of magnetic hybrid materials for efficient As (V) removal. *Chem. Eng. J.* **2016**, *301*, 83–91. [CrossRef]

52. Abdolali, A.; Ngo, H.H.; Guo, W.; Zhou, J.L.; Du, B.; Wei, Q.; Wang, X.C.; Nguyen, P.D. Characterization of a multi-metal binding biosorbent: Chemical modification and desorption studies. *Bioresour. Technol.* **2015**, *193*, 477–487. [CrossRef] [PubMed]
53. Lee, L.Y.; Lee, X.J.; Chia, P.C.; Tan, K.W.; Gan, S. Utilisation of Cymbopogon citratus (lemon grass) as biosorbent for the sequestration of nickel ions from aqueous solution: Equilibrium, kinetic, thermodynamics and mechanism studies. *J. Taiwan Inst. Chem. Eng.* **2014**, *45*, 1764–1772. [CrossRef]